J Biomol NMR (2009) 44:175–184
DOI 10.1007/s10858-009-9334-y

ARTICLE

Recoupling and decoupling of nuclear spin interactions at high MAS frequencies: numerical design of CN_n^v symmetry-based RF pulse schemes

Christian Herbst · Jirada Herbst · Anika Kirschstein · Jörg Leppert · Oliver Ohlenschläger · Matthias Görlach · Ramadurai Ramachandran

Received: 18 March 2009 / Accepted: 29 April 2009 / Published online: 23 June 2009
© Springer Science+Business Media B.V. 2009

Abstract The CN_n^v class of RF pulse schemes, commonly employed for recoupling and decoupling of nuclear spin interactions in magic angle spinning solid state NMR studies of biological systems, involves the application of a basic "*C*" element corresponding to an RF cycle with unity propagator. In this study, the design of CN_n^v symmetry-based RF pulse sequences for achieving ^{13}C–^{13}C double-quantum dipolar recoupling and through bond scalar coupling mediated ^{13}C–^{13}C chemical shift correlation has been examined at high MAS frequencies employing broadband, constant-amplitude, phase-modulated basic "*C*" elements. The basic elements were implemented as a sandwich of a small number of short pulses of equal duration with each pulse characterised by an RF phase value. The phase-modulation profile of the "*C*" element was optimised numerically so as to generate efficient RF pulse sequences. The performances of the sequences were evaluated via numerical simulations and experimental measurements and are presented here.

Keywords MAS · Solid state NMR · Chemical shift correlation · Symmetry-based RF pulse schemes

Electronic supplementary material The online version of this article (doi:10.1007/s10858-009-9334-y) contains supplementary material, which is available to authorized users.

C. Herbst · A. Kirschstein · J. Leppert · O. Ohlenschläger · M. Görlach · R. Ramachandran (✉)
Research Group Biomolecular NMR Spectroscopy, Leibniz Institute for Age Research, Fritz Lipmann Institute, 07745 Jena, Germany
e-mail: raman@fli-leibniz.de

J. Herbst
Department of Mathematics, Statistics and Computer, Faculty of Science, Ubon Ratchathani University, 34190 Ubon Ratchathani, Thailand

Introduction

Making use of the rotational properties of nuclear spin interactions and the application of rotor-synchronised RF pulse sequences, Levitt and co-workers have developed an elegant symmetry-based approach for recoupling weak dipolar interactions that are averaged out under magic-angle spinning conditions (Levitt 2002). Two classes of symmetry-based pulse sequences, denoted as CN_n^v and RN_n^v, have been introduced till date. The CN_n^v class of RF pulse schemes which is of interest in this study involves the application of a basic element "*C*" corresponding to an RF cycle with unity propagator $U_{RF}(\tau_c) = \pm 1$. *N* such cycles are applied over *n* rotor periods τ_r. Successive *C* elements are incremented in phase by $v2\pi/N$. *N*, *n* and *v* are all integers and appropriate values for these are chosen via the selection rules for CN_n^v and RN_n^v symmetry to generate the desired average Hamiltonian. The selection rule for the CN_n^v sequences states that the contributions to the lowest-order average Hamiltonian are zero unless $(mn - \mu v) = NZ$, where *Z* is any integer including zero and *m* and μ represent the spherical tensor components of the real and spin space parts A_{lm} and $T_{\lambda\mu}$ of the Hamiltonian, respectively. A variety of symmetries are available in principle for recoupling and decoupling of different nuclear spin interactions (Levitt 2002). The symmetry-based approach provides a very convenient platform for implementing different pulse schemes that are required, both in the context of resonance assignments and for obtaining structural constraints, in MAS solid state NMR studies of biological systems. For example, POST-C7 (Hohwy et al. 1998), the homonuclear double-quantum (DQ) recoupling scheme $C7_2^1$ with the basic *C* element $\{(\pi/2)_0(2\pi)_\pi(3\pi/2)_0\}$, is useful for generating ^{13}C–^{13}C chemical shift correlation data via longitudinal magnetisation exchange, double-quantum filtered

magnetisation transfers and double-quantum NMR spectroscopy (Heindrichs et al. 2000). It is worth noting that one of the limitations with symmetry-based RF pulse schemes based on conventional rectangular RF pulses is that the RF field strength requirements are related to the spinning speed (Karlsson et al. 2003). This can result in a situation where the RF field strength needed can become either too large which is beyond the hardware limits or too small leading to poor performance over a large bandwidth. Such difficulties restricting the applicability of symmetry-based pulse schemes can be overcome, in principle, by employing phase/amplitude modulated basic elements that are tailor made taking into account the experimental requirements and constraints such as available RF power and resonance offset range to be considered. In the context of side-chain ^{13}C resonance assignments in peptides and proteins such an approach was adopted in our recent study (Herbst et al. 2009) dealing with the implementation of scalar coupling mediated ^{13}C–^{13}C chemical shift correlation via the $C9^{1}_{15}$ symmetry scheme (Levitt 2002; Hardy et al. 2003) at a MAS frequency of 33.333 kHz. The basic element was constructed by concatenation of phase-modulated 180° pulses, e.g. $\{x\bar{x}\}$. Representing the phase modulation profiles of the 180° RF pulses in terms of a finite Fourier series, broadband 180° pulses were first generated via the iterative global optimisation procedure "genetic algorithms" (GA; Goldberg 1989; Forrest 1993; Judson 1997; Haupt and Haupt 2004; Freeman and Wu 1987; Wu and Freeman 1989; Xu et al. 1992). In the second step, the Fourier coefficients of the GA derived 180° pulses constituting the basic element were further optimised via the nonlinear least-squares optimisation procedure NL2SOL implemented in the SPINEVOLUTION program (Veshtort and Griffin 2006), so as to achieve, with the RF field strength available, the best possible performance of the symmetry-based scheme over the resonance offset range of the ^{13}C nuclei. One of the advantages with a Fourier series representation of the phase-modulation profile is that it typically involves only a small number of independent optimisation parameters and hence minimises the computational time required. Although a finite Fourier series representation of the phase-modulation profile of the RF pulses involved was found to lead to a satisfactory result, it has to be noted that such a representation restricts the solutions to only a small subset of all possible pulse profiles. Considering that the success of any local optimisation procedure such as the NL2SOL used in our study is dependent on the starting/initial parameter values, it will be advantageous to carry out the numerical calculation with a variety of potentially good starting input values such that different regions of the parameter space can be searched in finding the best possible solution. In this context, we have examined in this study an alternative approach for designing CN^{ν}_{n} symmetry-based schemes without significantly increasing the computational time. This exploits the fact that recoupling and decoupling of different nuclear spin interactions via the symmetry-based approach often involves the application of basic elements with a relatively short duration (Levitt 2002). For example, at a spinning speed of 25 kHz, homonuclear double-quantum (DQ) recoupling with suppression of CSA terms via the symmetries $C8^{3}_{10}$ and $C7^{2}_{10}$ would require, respectively, *C* elements with durations of 50.0 and 57.14 μs. Similarly, at a spinning speed of 33.333 kHz, the selection of homonuclear J-couplings with suppression of CSA and homonuclear dipolar interactions via the symmetry $C9^{1}_{15}$ requires a duration of 50 μs for the *C* element. This makes it possible to construct such basic *C* elements simply as a sandwich of a *small number* "N_t" of short pulses of equal duration and achieve satisfactory performance of the symmetry-based scheme by finding the optimal RF amplitude and phase values for each slice. In principle, the number of independent parameters, "N_i", defining the RF field modulation profile of the *C* element, can also be set smaller than N_t to reduce the computational time required in generating efficient symmetry-based RF pulse schemes. Employing such an approach, CN^{ν}_{n} symmetry-based RF pulse sequences for ^{13}C–^{13}C double-quantum dipolar recoupling and through bond scalar coupling mediated chemical shift correlation, under high-power ^{1}H decoupling during mixing, were generated at representative MAS frequencies using phase-modulated basic *C* elements of constant amplitude. Due to the fact that longer mixing times are typically required for TOBSY transfers, the ^{13}C and ^{1}H RF field interference effects during TOBSY mixing can be appreciable if sufficient mismatch between the ^{13}C and ^{1}H RF field strengths can not be achieved. Hence, TOBSY pulse schemes without simultaneous ^{1}H decoupling were also generated in this study. The performance characteristics of the sequences were assessed via numerical simulations and experimental measurements. The results from these investigations are reported here.

Numerical and experimental procedures

Basic *C* elements with appropriate duration, as determined by the symmetry and MAS frequency, were first generated either as a sandwich of two broadband inversion pulses, $\{x\bar{x}\}$, or directly as a broadband 2π pulse. Considering a simple spin 1/2 system, the global optimisation procedure "genetic algorithms" (GA) was employed in generating phase-modulated 180° and 360° pulses of constant amplitude so as to obtain, over the desired range of resonance offsets, the required response, $\langle I_z \rangle \rightarrow -\langle I_z \rangle$, and propagator, $\exp(i2\pi I_x)$, respectively. The GA program package GAlib (Wall 1996), as employed in our recent study

(Herbst et al. 2009), was used. Typically, a population size of 500 and 500 generations were used in the numerical calculations. The pulses were implemented as a sandwich of a small number of pulses of equal duration, typically in the range of 0.5–1.0 μs. RF field strengths employed were either in the range of 40–50 or 100–120 kHz depending on whether the pulses have to be used for implementing symmetry-based schemes with or without simultaneous ^{1}H decoupling. 180° pulses were constructed such that the phase modulation profile is symmetric with respect to the center of the pulse. The null rotation pulses were generated such that either the phase modulation profile is symmetric with respect to the center of the pulse (Type I) or the phase modulation profile of the first half of the pulse is 180° out of phase with respect to the second half and, additionally, the phase-modulation profile of each half was kept symmetric with respect to its center (Type II).

The GA derived C elements were used as the starting basic element in implementing different CN_n^{ν} symmetry-based pulse schemes. As the performance of the symmetry-based schemes with these C elements was far from satisfactory, the phase-modulation profiles of the C elements were further numerically optimised via the nonlinear least-squares optimisation procedure NL2SOL, as described below. The local optimisation run was repeated several times varying all the starting phase values randomly over a range of ±10%. These calculations were carried out neglecting RF field inhomogeneities and considering initially only a limited number of 32 crystallite orientations selected according to the Zaremba-Cheng-Wolfsberg (ZCW) method (Cheng et al. 1973). Starting with the solution thus obtained a final stage of optimisation was generally carried out considering a slightly larger number of crystallite orientations, typically 84. A Zeeman field strength corresponding to a ^{1}H resonance frequency of 500 MHz and representative spinning speeds were employed in this study. Typical chemical shift, scalar and dipolar coupling parameters of aliphatic carbons were used in the numerical design as in our earlier study (Herbst et al. 2009).

As representative examples, the symmetries $C7_{10}^{2}$ and $C8_{10}^{3}$ were examined for achieving γ-encoded ^{13}C–^{13}C DQ recoupling and the $C9_{15}^{1}$ symmetry was used for generating scalar coupling mediated ^{13}C–^{13}C chemical shift correlation (TOBSY; Baldus and Meier 1996; Agarwal and Reif 2008). Symmetry-based schemes with and without simultaneous application of ^{1}H decoupling were generated considering a two spin ^{13}C1–^{13}C2 and a four spin ^{1}H1–^{13}C1–^{13}C2–^{1}H2 system and a resonance offset range of ±10 and ±15 kHz, respectively. It is worth mentioning that the initial rate of transfer of magnetisation from one spin to another is a measure of the efficacy of the mixing sequence, with a faster transfer representing a more efficient dipolar or scalar coupling mediated magnetisation transfer. Considering this, in this study optimised RF pulse schemes were generated by monitoring the magnitude of longitudinal magnetisation transferred to the second carbon spin as a function of the mixing time, starting with z magnetisation on the first carbon spin at zero mixing time. It is seen via numerical simulations that with DQ recoupling sequences such as the POST-C7, the magnitude of the longitudinal magnetisation transferred to the second ^{13}C spin ($I_{1z} \rightarrow -I_{2z}$) typically reaches its maximum at ~1 ms, in a simple system of two directly coupled ^{13}C nuclei. Hence, at a representative spinning speed of 25 kHz, broadband DQ recoupling sequences were developed by maximising the magnitude of the longitudinal magnetisation transferred to the second ^{13}C spin at ~1 ms over the resonance offset range of the two nuclei. For TOBSY, considering a spinning speed of 33.333 kHz, the phase-modulation profile of the basic element employed in the $C9_{15}^{1}$ symmetry scheme was optimised so as to achieve complete magnetisation transfer from one carbon to another, ($I_{1z} \rightarrow I_{2z}$), at $\tau_{\mathrm{mix}} = (1/2J_{cc})$, over the resonance offset range of the two nuclei. The generation of the $C9_{15}^{1}$ symmetry-based pulse scheme for applications without simultaneous ^{1}H decoupling could not be effectively achieved via a single stage optimisation, considering the full ^{13}C–^{1}H dipolar coupling strength (set to 20 kHz, corresponding to a ^{13}C–^{1}H distance of ~1.14 Å). Hence, the ^{13}C–^{1}H dipolar coupling strength was raised gradually in several steps: 0, 2, 5, 10, 15 and 20 kHz, as in our earlier study. At every stage, to arrive at the best possible phase-modulation profile, the local optimisation run was repeated several times varying all the independent RF phase-values randomly over a range of ±10%. The best possible phase-modulation profile at the end of every stage was used as the starting input for the subsequent stage of optimisation.

All simulations to assess the performance characteristics of the pulse sequences were carried out with the SPINEVOLUTION program (Veshtort and Griffin 2006) considering 168 α and β powder angles selected according to the REPULSION scheme (Bak and Nielsen 1997) and 16 γ angles. Chemical shift correlation experiments via longitudinal magnetisation exchange were carried out via standard procedures using polycrystalline samples of (^{13}C,^{15}N) labelled histidine and arginine on a 500 MHz wide-bore Bruker Avance III solid state NMR spectrometer equipped with a 2.5 mm triple resonance probe with the cooling air kept at a temperature of ~50°C.

Results and discussion

Broadband, phase-modulated 180° and 360° pulses with required durations were generated via GA considering different bandwidths. Figures 1 and 2 show, as

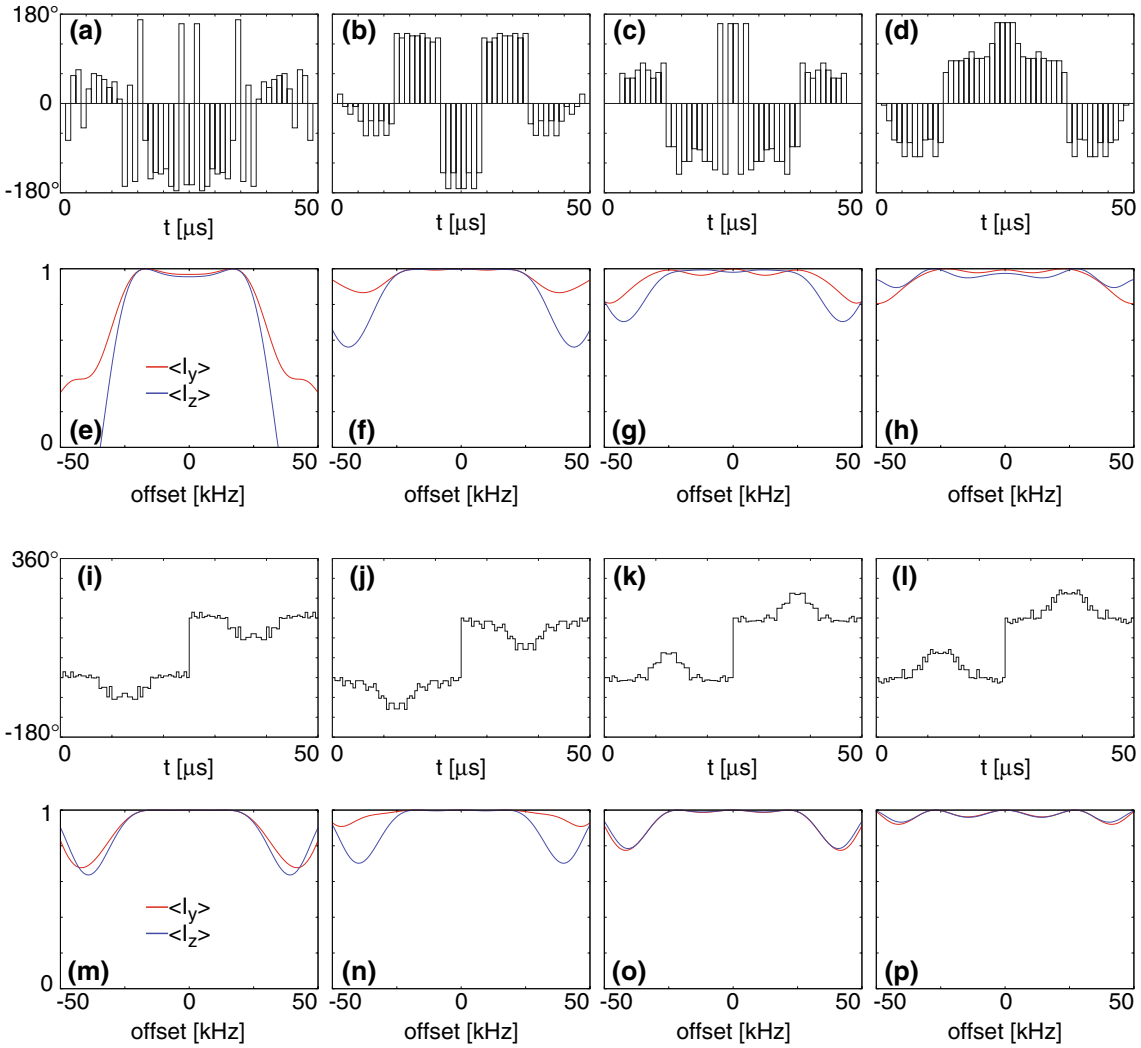

Fig. 1 RF phase values for the sandwich of 50 pulses of constant amplitude and equal duration constituting the 50 µs broadband 360° pulses (Type I) generated considering an RF field strength of 50 kHz and null rotation bandwidths of 40 kHz (**a**), 50 kHz (**b**), 60 kHz (**c**) and 70 kHz (**d**). The plots (**e**)–(**h**) show the response following the application of the different pulses, starting with I_z and I_y magnetisation components and considering a single spin-1/2 system. Plots (**i**)–(**l**) depict the RF phase modulation profiles of broadband 360° pulses (Type II) of constant amplitude and 50 µs duration generated as a sandwich of 100 pulses using an RF field strength of 50 kHz and null rotation bandwidths of 40 kHz (**i**), 50 kHz (**j**), 60 kHz (**k**) and 70 kHz (**l**). The plots (**m**)–(**p**) show the corresponding performance characteristics of the different null rotation pulses. The RF phase values for the first 25 slices are given in the supplementary material

representative examples, the phase-modulation profiles and the performance characteristics of some of the GA derived 2π pulses. Plots in Fig. 1a–h correspond to that of 360° pulses of 50 µs duration (Type I) generated with an RF field strength of 50 kHz and an N_t value of 50. Plots in Fig. 1i–p correspond to that of 360° pulses of 50 µs duration (Type II) generated with an RF field strength of 50 kHz and an N_t value of 100. Plots in Fig. 2a–h correspond to that of 360° pulses of 50 µs duration (Type I) generated with an RF field strength of 120 kHz and an N_t value of 50. Plots in Fig. 2i–p correspond to that of 360° pulses of 50 µs duration (Type II) generated with an RF field strength of 120 kHz and an N_t value of 100. Other details are given in the figure caption. Using a Mac Pro with four cores, typically, it was possible to generate these pulses in a very short time (<15 min). The performances of the pulses were found to be not affected significantly under minor variations in the RF field strength. The phase modulated pulses are scalable, as in the case of conventional pulses. A pulse applied for twice the duration would require half the RF field strength and correspondingly cover half the bandwidth of the original pulse. The simulated plots clearly demonstrate the potential of the GA approach for generating phase-modulated, broadband RF pulses simply as a sandwich of a small number of short pulses of equal duration with each slice characterised by a RF phase value. Considering that these pulses were only being used as the starting point of the numerical

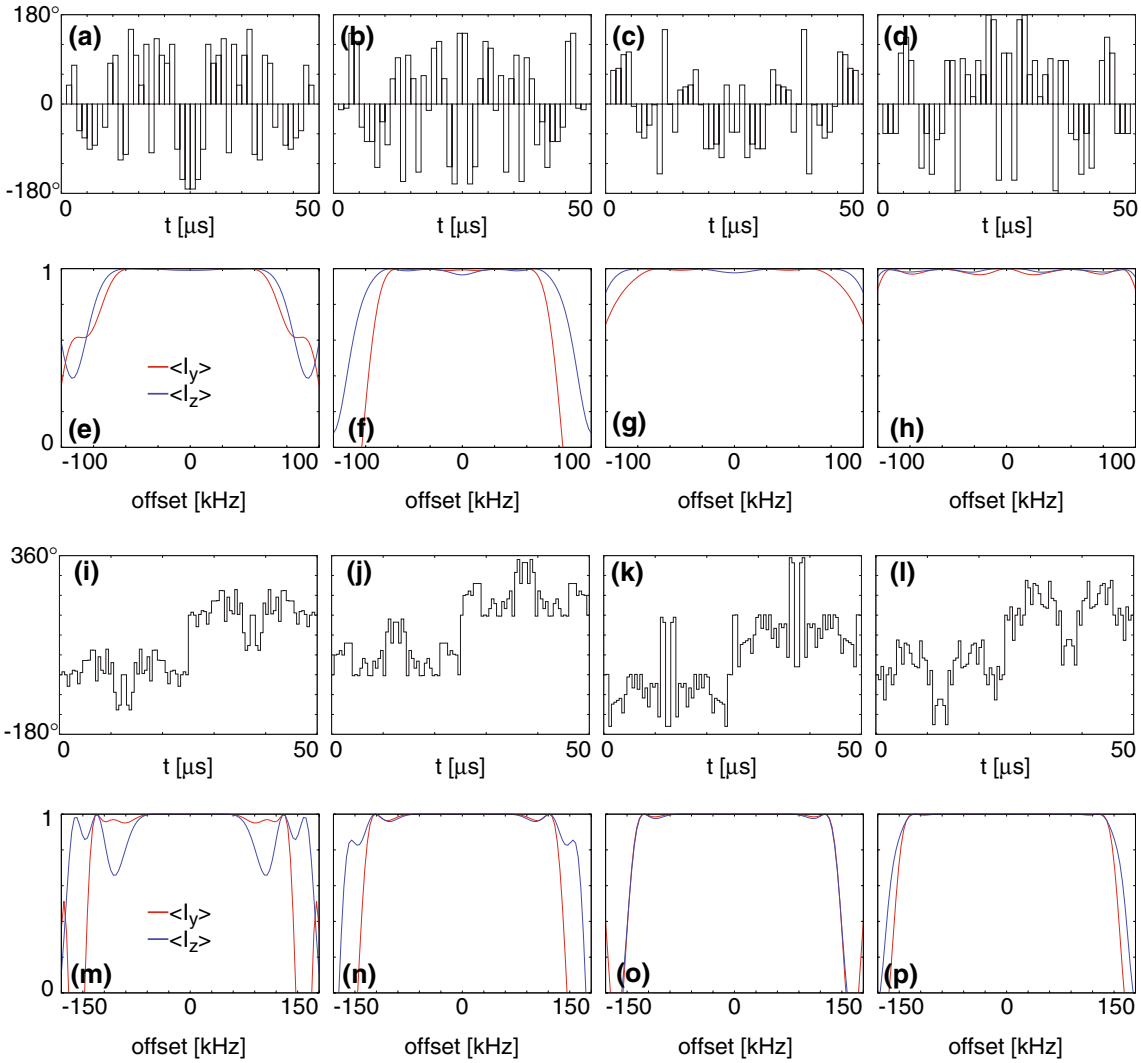

Fig. 2 RF phase values for the sandwich of 50 pulses of constant amplitude and equal duration constituting the 50 µs broadband 360° pulses (Type I) generated considering an RF field strength of 120 kHz and null rotation bandwidths of 60 kHz (**a**), 100 kHz (**b**), 140 kHz (**c**) and 180 kHz (**d**). The plots (**e**)–(**h**) show the corresponding performance characteristics of the different pulses, starting with I_z and I_y magnetisation components. Plots (**i**)–(**l**) depict the RF phase modulation profiles of broadband 360° pulses (Type II) of constant amplitude and 50 µs duration generated as a sandwich of 100 pulses using an RF field strength of 120 kHz and null rotation bandwidths of 60 kHz (**i**), 100 kHz (**j**), 140 kHz (**k**) and 180 kHz (**l**). The plots (**m**)–(**p**) show the corresponding performance characteristics of the different null rotation pulses. The RF phase values for the first 25 slices are given in the supplementary material

optimisation procedure, no attempts were made to generate RF pulses with better performance characteristics, e.g. by optimising the population size and the number of generations.

Starting with different GA derived *C* elements, a large number of numerical optimisation runs were carried out for realising satisfactory performance of the chosen symmetry-based scheme. In general it was possible to generate, for each symmetry, a variety of optimised basic elements that lead to the satisfactory performance of the pulse sequence. Using a Mac Pro with four cores, typically, it was possible to generate CN_n^ν symmetry-based schemes in a short time (<3 h). The simulated performance characteristics of the numerically designed $C7_{10}^2$ and $C8_{10}^3$ symmetries are shown in Fig. 3 along with the phase-modulation profiles (a, d) of the basic *C* elements [null rotation pulse (Type I)]. The plots (b, e) show as a function of the mixing time the magnitude of longitudinal magnetisation transferred to the second carbon spin. These plots were obtained using the chemical shift tensor and dipolar coupling parameters of alanine and glycine, with the ^{13}C carrier kept either at the center of the two resonances or at 110 ppm, as indicated. Although the optimised basic elements were generated employing CSA, scalar and dipolar coupling parameters corresponding to that of the $^{13}C^\alpha$ and $^{13}C^\beta$ nuclei of alanine, it is seen that reasonably satisfactory performance can

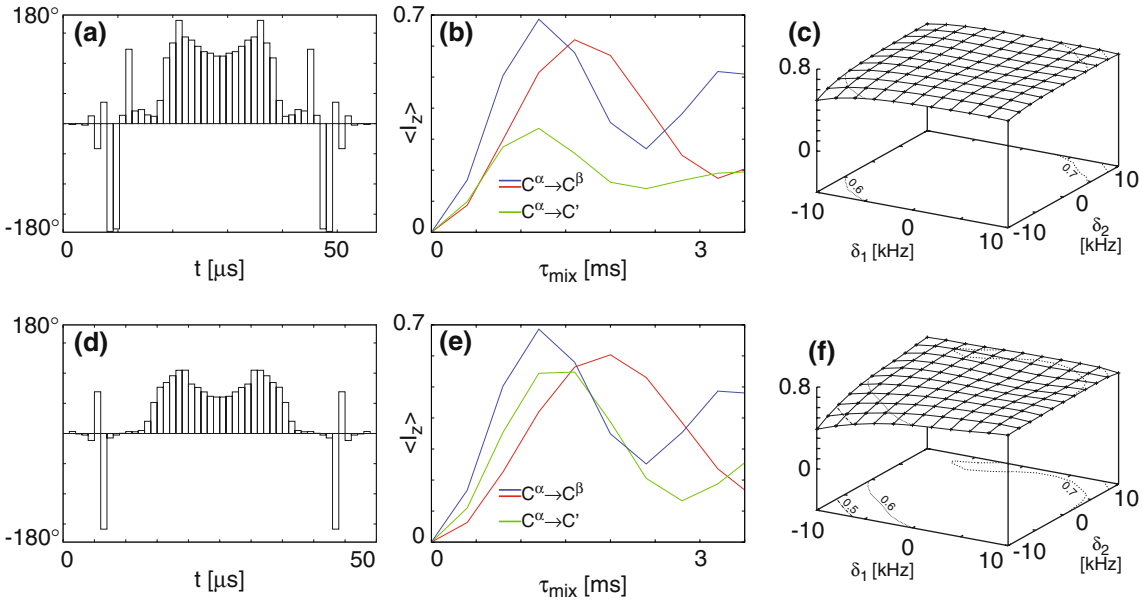

Fig. 3 Simulated longitudinal magnetisation transfer characteristics of the $C7^2_{10}$ (**a**, **b**, **c**) and $C8^3_{10}$ (**d**, **e**, **f**) symmetries along with the phase-modulation profiles (**a**, **d**) of the basic *C* elements of duration 57.14 and 50 μs, respectively. Simulations were carried out at a spinning speed of 25 kHz, for a Zeeman field strength corresponding to a ^{1}H resonance frequency of 500 MHz and with RF field strengths of 44 kHz (**b**, **c**) and 45 kHz (**e**, **f**) during mixing. The simulated plots (**b**, **e**) show the magnitude of the transferred magnetisation (normalised to the maximum transferable signal) on the second carbon starting with *z* magnetisation on carbon 1. The simulations for the $C^\alpha \rightarrow C^\beta$ and $C^\alpha \rightarrow C'$ transfers were carried out using typical chemical shift, scalar and dipolar coupling parameters of alanine and glycine with the ^{13}C carrier kept either at the center of the two resonances (plot shown in *blue*) or at 110 ppm (*green* and *red*). Plots given in (**c**) and (**f**) show, as a function of the resonance offsets of the dipolar coupled nuclei, the magnitude of the transferred magnetisation on spin 2 at a τ_{mix} of 1.2 ms, starting with *z* magnetisation on the first carbon spin at zero mixing time. The RF phase values for the first 25 slices of the basic *C* elements are given in the supplementary material

also be obtained even in the situation where one of the carbons has a large CSA, as in the case of the $^{13}C^\alpha \rightarrow {}^{13}C'$ magnetisation transfer in peptides and proteins. At moderate Zeeman field strengths, the plots in Fig. 3b, e suggest that it may be even possible to achieve satisfactory DQ recoupling in the entire ^{13}C spectral range. Plots given in Fig. 3c, f show, as a function of the resonance offsets of the dipolar coupled nuclei, the magnitude of the transferred magnetisation on spin 2 at a τ_{mix} of 1.2 ms, starting with *z* magnetisation on the first carbon spin at zero mixing time. It is seen that the performance characteristics of the sequences are not very much dependent on the resonance offsets of the dipolar coupled nuclei. The data shown in Fig. 3 indicate that it is possible to achieve, even at high MAS frequencies, satisfactory DQ recoupling using only a moderate ^{13}C RF field strength of 50 kHz or less. It is worth mentioning that, employing the symmetries $C7^2_{10}$ and $C8^3_{10}$ and using an ^{13}C RF field strength of $\sim$50 kHz, we have also achieved satisfactory DQ recoupling at the spinning speed of 25 kHz using phase-modulated basic *C* elements where the RF phase-modulation profile was defined in terms of a finite Fourier series (see supplementary material). The performances of these sequences were found to be comparable to that shown in Fig. 3.

Starting with a variety of basic *C* elements, TOBSY optimisation calculations were carried out with the $C9^1_{15}$ symmetry considering an RF field strength of 50 kHz, spinning speed of 33.333 kHz and a resonance offset range of $\pm$10 kHz. In this case, null rotation pulses of Type II were found to lead to satisfactory solutions. The phase-modulation profile of one of the basic *C* elements generated in this study using CSA, scalar and dipolar coupling parameters corresponding to that of the $^{13}C^\alpha$ and $^{13}C^\beta$ nuclei of alanine are given in Fig. 4a. The simulated magnetisation transfer characteristics given in Fig. 4b indicate that the $C9^1_{15}$ symmetry with the numerically optimised basic elements can be effectively employed for TOBSY experiments in the aliphatic region of peptides and proteins. The performance observed using CSA, scalar and dipolar coupling parameters corresponding to that of $^{13}C^\alpha$ and $^{13}C'$ nuclei of glycine, however, were found to be not satisfactory (data not shown). The plot given in Fig. 4c shows, as a function of the resonance offsets of the scalar coupled nuclei, the magnitude of the transferred magnetisation on spin 2 at a τ_{mix} of $\sim$14 ms, starting with *z* magnetisation on the first carbon spin at zero mixing time. It is observed that the performance characteristics of the sequence is not very much dependent on the resonance

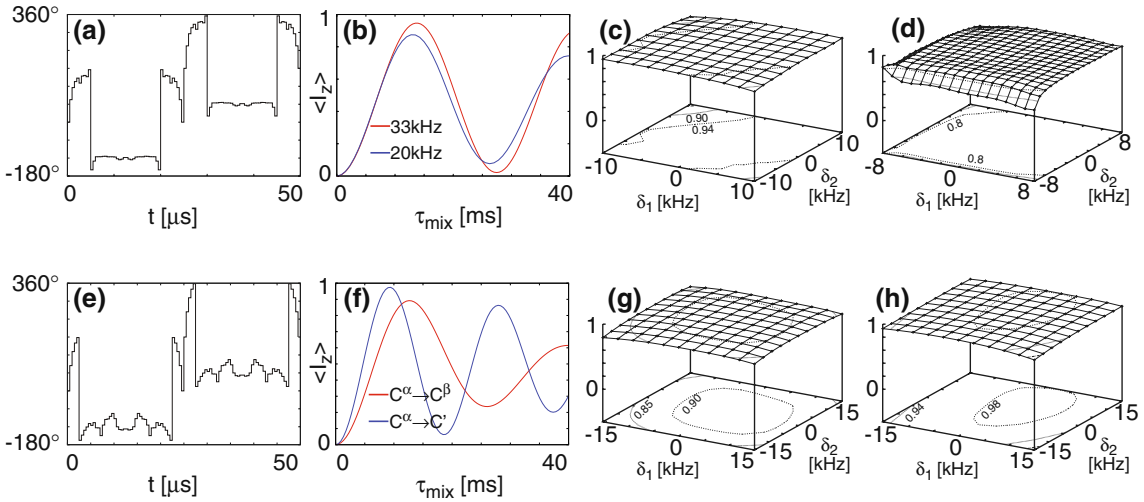

Fig. 4 Simulated longitudinal magnetisation transfer characteristics observed with the $C9^{1}_{15}$ symmetry-based RF pulse scheme. The optimised phase-modulation profile of the basic *C* element of 50 μs duration shown in (**a**) was generated considering an RF field strength of 50 kHz and a spinning speed of 33.333 kHz. The simulated plots given in (**b**) show the magnitude of the transferred magnetisation (normalised to the maximum transferable signal) on the second carbon starting with *z* magnetisation on carbon 1. These were generated using typical chemical shift, scalar and dipolar coupling parameters of alanine, with the ^{13}C carrier kept at the center of the two resonances. The magnetisation transfer plot at a spinning speed of 20 kHz was obtained using the same phase-modulation profile as in (**a**) using an RF field strength of 30 kHz and a C element duration of 83.33 μs. The plots given in (**c**) and (**d**) show, as a function of the resonance offsets of the scalar coupled nuclei, the magnitude of the transferred magnetisation on spin 2 at a τ_{mix} of ~14 ms, starting with *z* magnetisation on the first carbon spin at zero mixing time. The optimised phase-modulation profile of the basic *C* element of 50 μs duration shown in (**e**) was generated considering an RF field strength of 120 kHz and a spinning speed of 33.333 kHz. The simulated plots in (**f**) show, at a Zeeman field strength corresponding to a ^{1}H frequency of 500 MHz, the magnitude of the transferred magnetisation (normalised to the maximum transferable signal) on the second carbon ($^{13}C^{\beta}/^{13}C'$) starting with *z* magnetisation on carbon 1 ($^{13}C^{\alpha}$). The simulations for the $C^{\alpha} \rightarrow C^{\beta}$ transfer were carried out considering a four spin $^{1}H1–^{13}C1–^{13}C2–^{1}H2$ network (with all the atoms in the same plane) and those for the $C^{\alpha} \rightarrow C'$ transfer were carried out with a three spin $^{1}H1–^{13}C1–^{13}C2$ network. A $^{13}C–^{1}H$ dipolar coupling strength of 20 kHz was employed in these simulations and the C–H bonds were assumed to be at an angle of 109° with respect to the C–C bond. These simulations were carried out keeping the ^{13}C RF carrier at 110 ppm, using typical chemical shift, scalar and dipolar coupling parameters of alanine and glycine as in our earlier studies. The plots given in (**g**) and (**h**) correspond, respectively, to $C^{\alpha} \rightarrow C^{\beta}$ and $C^{\alpha} \rightarrow C'$ magnetisation transfers. They show, as a function of the resonance offsets of the scalar coupled nuclei, the magnitude of the transferred magnetisation on spin 2 at a τ_{mix} of ~14 and 9.5 ms, respectively, starting with *z* magnetisation on the first carbon spin at zero mixing time. The RF phase values for the first 25 slices of the basic *C* elements are given in the supplementary material

offsets of the two nuclei. For a given symmetry, to get the best possible performance it is generally advantageous to numerically optimise the RF pulse characteristics of the basic *C* element taking into consideration the spinning speed to be employed. However, in many situations it may be possible to employ the same basic element at different MAS frequencies, using appropriately scaled pulse widths and RF field strengths, and still obtain satisfactory TOBSY performance. For example, the performance of the $C9^{1}_{15}$ symmetry using the same basic element given in Fig. 4a is found to be not significantly affected at a spinning speed of 20 kHz (Fig. 4b, d) and the bandwidth over which efficient TOBSY magnetisation transfer can be realised is still sufficiently large enough to cover the entire aliphatic ^{13}C spectral range of peptides and proteins.

The TOBSY magnetisation transfer characteristics observed with the $C9^{1}_{15}$ symmetry-based scheme, without ^{1}H decoupling during mixing, at a spinning speed of 33.333 kHz and using an RF field strength of 120 kHz, and the corresponding optimised basic C element are shown in Fig. 4e–h. The 1D magnetisation transfer plots (Fig. 4f) were obtained keeping the ^{13}C RF carrier at 110 ppm. 3D plots given in 4 g and 4 h show the magnetisation transfer characteristics as a function of the resonance offsets of the two nuclei involved. The plot given in Fig. 4g was obtained considering a four-spin $^{1}H1–^{13}C1–^{13}C2–^{1}H2$ system and employing CSA, scalar and dipolar coupling parameters corresponding to that of the $^{13}C^{\alpha}$ and $^{13}C^{\beta}$ nuclei of alanine. The plot given in Fig. 4h was obtained considering a three-spin $^{1}H1–^{13}C1–^{13}C2$ system and using CSA, scalar and dipolar coupling parameters corresponding to that of $^{13}C^{\alpha}$ and $^{13}C'$ nuclei of glycine. Although the optimised basic element was generated employing CSA, scalar and dipolar coupling parameters corresponding to that of the $^{13}C^{\alpha}$ and $^{13}C^{\beta}$ nuclei of alanine, it is seen that satisfactory performance can be obtained even in the case of the $^{13}C^{\alpha} \rightarrow {}^{13}C'$ magnetisation transfer. The performance of the $C9^{1}_{15}$ symmetry-based scheme employing the numerically optimised phase-modulated basic "*C*" element generated in this study is seen to be comparable to that

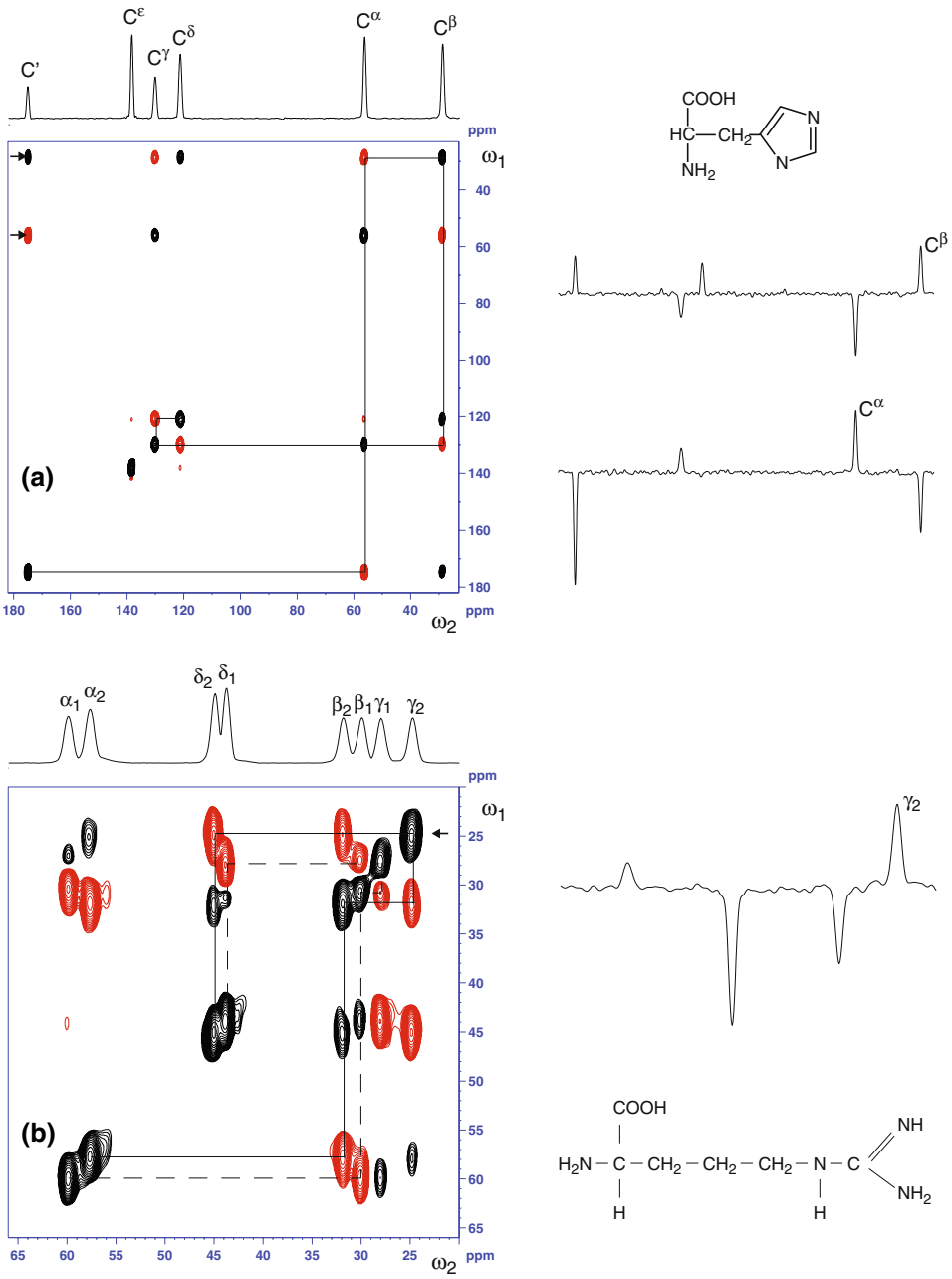

Fig. 5 2D ^{13}C–^{13}C chemical shift correlation spectra of L-histidine hydrochloride (**a**) and L-arginine hydrochloride (**b**) obtained via longitudinal magnetisation transfer at a spinning speed of 25 kHz using $C7^2_{10}$ (**a**) and $C8^3_{10}$ (**b**) DQ dipolar recoupling schemes. These spectra were obtained employing a mixing time of 1.2 ms, the corresponding numerically optimised basic *C* elements given in Fig. 3 and appropriate ^{13}C RF field strengths. The spectra were generated with 32 transients per t_1 increment, 64 t_1 increments, spectral width in the indirect dimension of 25,000 Hz and recycle time of 2 s (**a**) and 4 s (**b**), keeping the RF carrier at 100 ppm. Fig. 5b shows the zoomed plot of the aliphatic region [Two resonances are seen for each of the arginine aliphatic carbons, due to the presence of two different crystal forms (Baldus and Meier 1996)]. A few representative cross-sections are also given to indicate spectral quality

obtained in our earlier investigation (Herbst et al. 2009) where the RF phase-modulation profile was defined in terms of a finite Fourier series. It is worth mentioning that, at the expense of more computational time, it may also be possible to numerically design symmetry-based schemes via alternative procedures such as optimal control theory based algorithms (Kobzar et al. 2004) employing randomly generated phase values for the RF field modulation profile.

The performance characteristics of the symmetry-based sequences reported here were also assessed via experimental measurements and some representative data are given below. The ^{13}C–^{13}C chemical shift correlation spectra of polycrystalline samples of histidine and arginine, acquired employing the $C7^2_{10}$ and $C8^3_{10}$ symmetries, respectively, at a spinning speed of 25 kHz using the numerically optimised phase-modulated basic elements are shown in Fig. 5a, b, along with a few cross-sections to indicate the spectral quality. As reflected by the corresponding crosspeak intensities, significant relayed magnetisation transfers are seen even at the short τ_{mix} employed. As expected under DQ mixing, the spectra and the spectral cross-sections clearly show the characteristic alternation of direct and relayed cross-peak intensities. The TOBSY spectra of the aliphatic region of arginine shown in Fig. 6a, b were generated with the $C9^1_{15}$ symmetry, at a spinning speed of 20 kHz, using the numerically optimised phase-modulated basic element

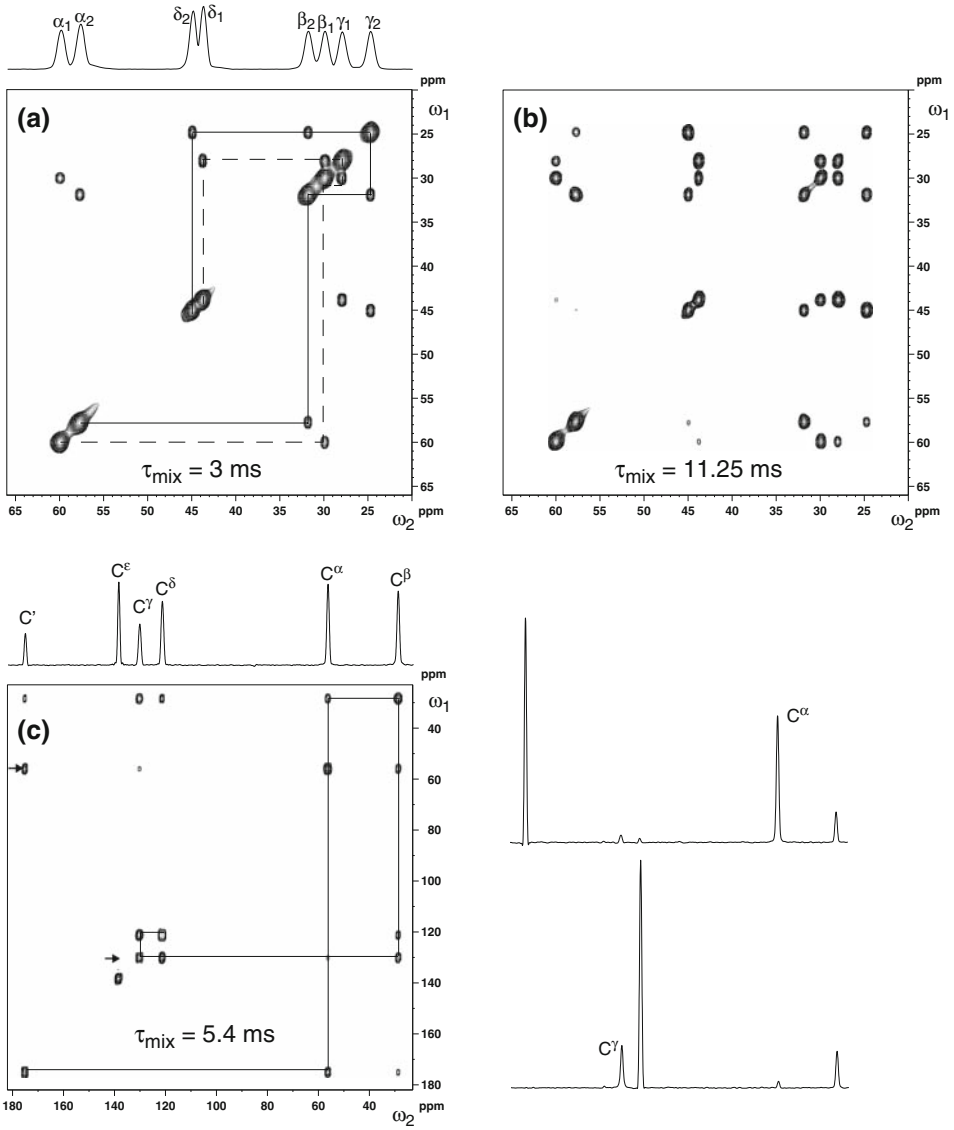

Fig. 6 2D ^{13}C–^{13}C scalar coupling mediated chemical shift correlation spectra of L-arginine hydrochloride (**a**, **b**) and L-histidine hydrochloride (**c**). Spectra (**a**) and (**b**) were obtained at a spinning speed of 20.0 kHz, with ^{13}C RF field strength of 30 kHz during mixing and using mixing times of 3 ms (**a**) and 11.25 ms (**b**), employing the $C9^1_{15}$ symmetry-based RF pulse scheme, using a basic *C* element with the optimised phase-modulation profile given in Fig. 4a, 48 transients per t_1 increment, 64 t_1 increments, spectral width in the indirect dimension of 10,000 Hz, recycle time of 4 s and with the RF carrier kept at 40 ppm. The base contour level in (**b**) was set at half the value used in (**a**). Spectrum (**c**) was obtained with the $C9^1_{15}$ symmetry-based RF pulse scheme and the basic *C* element given in Fig. 4e without ^1H decoupling during mixing, at a spinning speed of 33.333 kHz, with ^{13}C RF field strength of 120 kHz during mixing, a mixing time of 5.4 ms, 16 transients per t_1 increment, 128 t_1 increments, spectral width in the indirect dimension of 33.333 kHz, recycle time of 2 s and with the RF carrier kept at 100 ppm. A few representative cross-sections are also given to indicate spectral quality

shown in Fig. 4a and with mixing times of 3.0 ms (6a) and 11.25 ms (6b). Direct and relayed cross-peaks of appreciable intensities could be clearly seen in the spectra. Spectrum 6c was obtained at a spinning speed of 33.333 kHz with the $C9^1_{15}$ symmetry-based RF pulse scheme and the basic *C* element given in Fig. 4e without ^1H decoupling during mixing. Consistent with the results from numerical simulations, it is seen that CN^v_n symmetry-based TOBSY and DQ recoupling schemes can be effectively implemented for the study of isotopically labelled biological systems at fast MAS frequencies.

In conclusion, the present study demonstrates an approach for exploiting the full potential of the symmetry-based procedure for implementing different RF pulse sequences that are commonly required in the study of biological systems. For the recoupling and decoupling of the relevant nuclear spin interactions, it has been the common practice to examine the performance of a variety of allowed symmetries using different composite pulse based basic elements. In contrast to this, it is seen from our study that it is possible to tailor the characteristics of the basic element for each symmetry so as to realise the best possible performance of the chosen symmetry. The method outlined here makes use of basic "*C*" elements, implemented as a sandwich of a small number of short pulses of equal duration with each pulse characterised by a RF phase value, for constructing CN^v_n symmetry-based RF pulse sequences. Optimisation of the phase-modulation profile of the basic elements is shown to permit the generation of symmetry-based RF pulse schemes with satisfactory magnetisation transfer characteristics. While in our earlier study we used a finite Fourier series representation of the phase-modulation profile of basic "*C*" elements, the method outlined here provides an alternative approach for

searching different regions of the parameter space for finding the best possible solution and is especially suited in situations where basic "*C*" elements with relatively short durations are required. As seen from the present study, efficient symmetry-based schemes could be designed with basic "*C*" elements implemented with only a limited number of independent phase variables. Hence, to minimise computational time, it will be advantageous to start the search for optimal solutions using only a small number of optimisation parameters. Only in situations where satisfactory solutions can not be obtained, we believe that it is necessary to carry out the calculations with a larger number of optimisation parameters, either by increasing the total number of slices or by using asymmetric phase-modulation profiles of the "*C*" element. Although RF field inhomogeneities were not considered explicitly, the symmetry-based schemes reported here have been found, via numerical simulations, to have reasonable tolerance to such imperfections. Considering that the success of any local numerical optimisation procedure is dependent on the starting/initial parameter values, the present study shows the possibilities for generating a variety of basic "*C*" elements using global optimisation procedures such as GA. Although only nominal CSA values and simple spin systems were considered in this study, the method outlined here can be easily adapted, where required, for implementing RF pulse sequences considering different CSA parameters and spin networks. The present approach can also be extended for implementing RN_n^{ν} symmetry-based pulse sequences, with or without simultaneous ^{1}H decoupling.

Acknowledgments This study has been funded in part by a grant from the Deutsche Forschungsgemeinschaft (GO474/6-1). The FLI is a member of the Science Association 'Gottfried Wilhelm Leibniz' (WGL) and is financially supported by the Federal Government of Germany and the State of Thuringia.

References

Agarwal V, Reif B (2008) Residual methyl protonation in perdeuterated proteins for multi-dimensional correlation experiments in MAS solid-state NMR spectroscopy. J Magn Reson 194:16–24

Bak M, Nielsen NC (1997) REPULSION, a novel approach to efficient powder averaging in solid state NMR. J Magn Reson 125:132–139

Baldus M, Meier BH (1996) Total correlation spectroscopy in the solid state. The use of scalar couplings to determine the through-bond connectivity. J Magn Reson A 121:65–69

Cheng VB, Suzukawa HH, Wolfsberg M (1973) Investigations of a nonrandom numerical method for multidimensional integration. J Chem Phys 59:3992–3999

Forrest S (1993) Genetic algorithms-principles of natural-selection applied to computation. Science 261:872–878

Freeman R, Wu XL (1987) Design of magnetic resonance experiments by genetic evolution. J Magn Reson 75:184–189

Goldberg DE (1989) Genetic algorithms in search, optimization and machine learning. Addison-Wesley publishing company, Massachusetts

Hardy EH, Detken A, Meier BH (2003) Fast-MAS total through-bond correlation spectroscopy using adiabatic pulses. J Magn Reson 165:208–218

Haupt RL, Haupt SE (2004) Practical genetic algorithms. Wiley-Interscience, New Jersey

Heindrichs ASD, Geen H, Titman JJ (2000) MAS double-quantum filtered dipolar shift correlation spectroscopy. J Magn Reson 147: 68–77

Herbst C, Herbst J, Kirschstein A, Leppert J, Ohlenschläger O, Görlach M, Ramachandran R (2009) Design of high-power, broadband 180° pulses and mixing sequences for fast MAS solid state chemical shift correlation NMR spectroscopy. J Biomol NMR 43:51–61

Hohwy M, Jakobsen HJ, Eden M, Levitt MH, Nielsen NC (1998) Broadband dipolar recoupling in the nuclear magnetic resonance of rotating solids: a compensated C7 pulse sequence. J Chem Phys 108:2686–2694

Judson R (1997) Genetic algorithms and their use in chemistry. In: Lipkowitz KB, Boyd DB (eds) Reviews in computational chemistry, vol 10. VCH Publishers, New York, pp 1–73

Karlsson T, Popham JM, Long JR, Oyler N, Drobny GP (2003) A study of homonuclear dipolar recoupling pulse sequences in solid-state nuclear magnetic resonance. J Am Chem Soc 125:7394–7407

Kobzar K, Skinner TE, Khaneja N, Glaser SJ, Luy B (2004) Exploring the limits of broadband excitation and inversion pulses. J Magn Reson 170:236–243

Levitt MH (2002) Symmetry-based pulse sequences in magic-angle spinning solid-state NMR. In: Grant DM, Harris RK (eds) Encyclopedia of nuclear magnetic resonance. Wiley, Chichester

Veshtort M, Griffin RG (2006) SPINEVOLUTION: a powerful tool for the simulation of solid and liquid state NMR experiments. J Magn Reson 178:248–282

Wall M (1996) GAlib: a C++ library of genetic algorithm components, version 2.4.7. http://lancet.mit.edu/ga/

Wu XL, Freeman R (1989) Darwin's ideas applied to magnetic resonance. The marriage broker. J Magn Reson 85:414–420

Xu P, Wu XL, Freeman R (1992) User-friendly selective pulses. J Magn Reson 99:308–322